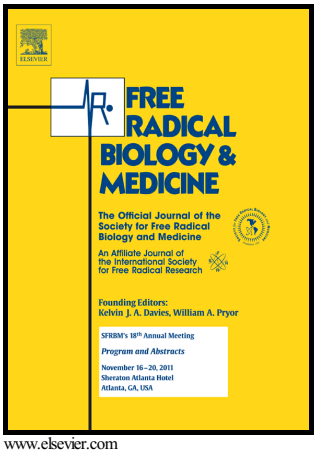

www.elsevier.com

Pro-fluorescent mitochondria-targeted real-time responsive redox probes synthesised from carboxy isoindoline nitroxides: Sensitive probes of mitochondrial redox status in cells

Kok Leong Chong, Benjamin A. Chalmers, Jason K. Cullen, Amandeep Kaur, Jacek L. Kolanowski, Benjamin J. Morrow, Kathryn E. Fairfull-Smith, Martin J. Lavin, Nigel L. Barnett, Elizabeth J. New, Michael P. Murphy, Steven E. Bottle

PII: S0891-5849(18)30112-6
DOI: https://doi.org/10.1016/j.freeradbiomed.2018.03.008
Reference: FRB13655

To appear in: *Free Radical Biology and Medicine*

Received date: 29 November 2017
Revised date: 12 February 2018
Accepted date: 6 March 2018

Cite this article as: Kok Leong Chong, Benjamin A. Chalmers, Jason K. Cullen, Amandeep Kaur, Jacek L. Kolanowski, Benjamin J. Morrow, Kathryn E. Fairfull-Smith, Martin J. Lavin, Nigel L. Barnett, Elizabeth J. New, Michael P. Murphy and Steven E. Bottle, Pro-fluorescent mitochondria-targeted real-time responsive redox probes synthesised from carboxy isoindoline nitroxides: Sensitive probes of mitochondrial redox status in cells, *Free Radical Biology and Medicine,* https://doi.org/10.1016/j.freeradbiomed.2018.03.008

Pro-fluorescent mitochondria-targeted real-time responsive redox probes synthesised from carboxy isoindoline nitroxides: Sensitive probes of mitochondrial redox status in cells

Kok Leong Chong[a], Benjamin A. Chalmers[a], Jason K. Cullen[b], Amandeep Kaur[c], Jacek L. Kolanowski[c], Benjamin J. Morrow[a], Kathryn E. Fairfull-Smith[a], Martin J. Lavin[b,d], Nigel L. Barnett[e], Elizabeth J. New[c], Michael P. Murphy[f] and Steven E. Bottle[a]*

[a]ARC Centre of Excellence for Free Radical Chemistry, Faculty of Science and Engineering, Queensland University of Technology (QUT), Brisbane, Queensland, Australia.
[b]Cell and Molecular Biology, Queensland Institute of Medical Research, Brisbane, Australia
[c]School of Chemistry, University of Sydney
[d]University of Queensland, Centre for Clinical Research, Brisbane, Australia
[e]Queensland Eye Institute, South Brisbane, Australia
[f]MRC Mitochondrial Biology Unit, University of Cambridge, Cambridge CB2 0XY, UK

Abstract

Here we describe new fluorescent probes based on fluorescein and rhodamine that provide reversible, real-time insight into cellular redox status. The new probes incorporate bio-imaging relevant fluorophores derived from fluorescein and rhodamine linked with stable nitroxide radicals such that they cannot be cleaved, either spontaneously or enzymatically by cellular processes. Overall fluorescence emission is determined by reversible reduction and oxidation, hence the steady state emission intensity reflects the balance between redox potentials of critical redox couples within the cell. The permanent positive charge on the rhodamine-based probes leads to their rapid localisation within mitochondria in cells. Reduction and oxidation also leads to marked changes in the fluorophore lifetime, enabling monitoring by fluorescence lifetime imaging microscopy. Finally, we demonstrate that administration of a methyl ester version of the rhodamine-based probe can be used at concentrations as low as 5 nM to generate a readily detected response to redox stress within cells as analysed by flow cytometry.

Key Words

Nitroxide

Fluorescent probe

Mitochondria

Redox Status

Oxidative Stress

Introduction

Nitroxide free radicals, or more correctly aminoxyls, have been known for more than 170 years and can act as antioxidants, either directly or after conversion to a hydroxylamine. The first reported example of a nitroxide free radical was that of Frémy's salt, which was synthesised in 1845 [1]. Although it is likely that there were nitroxides generated in Piloty's reactions of potassium cyanide with isobutyramidine in the early 1900s [2], it would take a further 50 years and the development of magnetic resonance spectroscopy before the work of Lebedev [3] and later Henderson [4] sparked a remarkable period where nitroxides, spin labels and spin trapping generated insight into materials science, structural biology and the understanding of reactive intermediates. As nitroxides are stable towards many solvents and reagents as well as the atmosphere, while possessing an unpaired spin that rapidly scavenges reactive free radicals, they were quickly exploited as potent antioxidants. Even today, modern "plastics" contain significant levels of hindered amine stabilisers that are precursors to nitroxides [5], thereby retarding oxidation and extending application lifetimes. In free radical biology it was rapidly determined that nitroxides interact with superoxide *in vitro* [6] acting as superoxide dismutase mimetics [7], as they reproduce some of the impact of those enzymes that degrade superoxide. However, for kinetic reasons, the antioxidant effects reported for nitroxides *in vivo* most likely follow their rapid metabolic conversion to hydroxylamines [8]. The remarkable chemistry of nitroxides arises from them being persistent entities existing in between less stable one-electron reduction and one-electron oxidation products, each of which can be accessed at biologically relevant redox potentials (Figure **1A**.).

A.

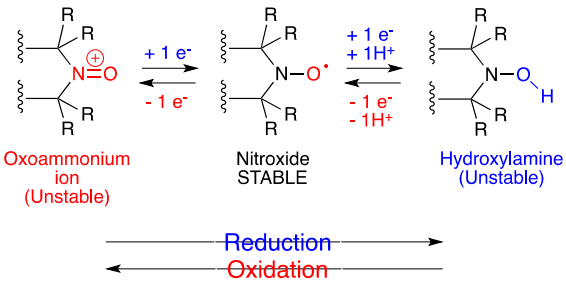

B.

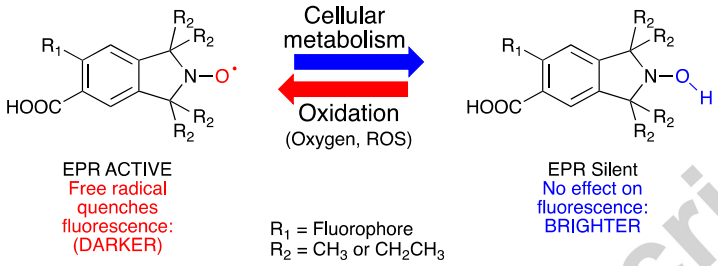

C.

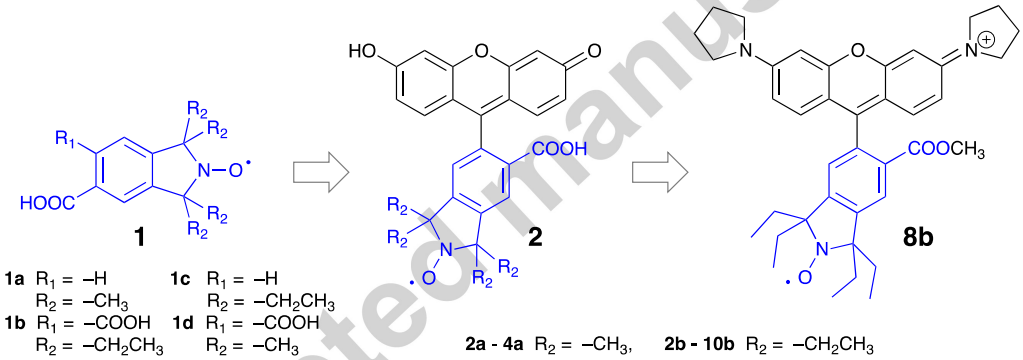

Figure 1. A. Nitroxides exist at an oxidation state between more oxidised (oxoammoninium ions) and more reduced (hydroxylamine) forms. **B.** When exposed to living systems nitroxides are reduced to non-radical hydroxylamines. This transformation is reversed in the presence of oxygen and other oxidising species including many reactive oxygen species (ROS). The steady state level of nitroxides can be monitored by EPR, or by fluorescence when fluorophores are incorporated within the structure. **C.** Carboxyisoindoline nitroxides (**1**) serve as precursors for fluorescein-based pro-fluorescent nitroxides (**2**) and rhodamine-based nitroxides (**5** and **8**)

Subtleties in the chemical structure, including the ring size, type and substitution influence these redox potentials [9]. However, it is important to note that, despite being known as antioxidants, most nitroxides exposed to living systems, are *reduced* to the non-radical hydroxylamine [10]. This demonstrates that, within a living system, nitroxides are treated as oxidants, requiring cells to use some of their

reductive capacity to reduce the nitroxide to the non-radical species. Whilst this rapid reduction leads to signal loss and limits electron paramagnetic resonance (EPR) imaging, it also presents a unique means to assess the redox state of redox couples within living systems that interact with nitroxides and their reduced and/or oxidised products. More rapid reduction of the nitroxide represents functional reducing capacity, whereas slower reduction reflects compromised reducing capacity, which may indicate disease and consequent cellular dysfunction. Complicating the situation is oxygen, which can re-oxidise the hydroxylamine back to the nitroxide. Thus, the steady-state amount of nitroxide present in a living system depends on a range of factors including: the ease of oxidation of the hydroxylamine; the concentration and nature of oxidising species; the speed of the reduction of the nitroxide; the localisation of the nitroxide within the cell; the polarity/lipophilicity and charge of the molecule; and also the ease with which nitroxides can interact with reductive enzymes and other biologically relevant reducing agents such as ascorbate, ubiquinol and, indirectly, glutathione. Importantly this *reversibility* of nitroxide oxidation and reduction imparts an advantage to the use of nitroxides as biological probes. A probe that establishes a paramagnetic/diamagnetic equilibrium in response to local conditions within a biological system will respond to, in real-time and reversibly, the overall redox status of cognate redox couples within the cellular system being investigated and will respond in real time to any changes to these couples, such as those in response to pathology, drugs and environmental stresses (Figure **1B**.). However it is important to note that these responses will be dominated by the entirety of the biological milieu and that there is not one "redox couple" or "redox state" reported on by these probes.

In an earlier attempt to exploit these properties we designed [11] a structurally efficient fluorescein-based, dual mode fluorescent probe (Figure **1C**.: **2a.** $R_2 = -CH_3$) designed to respond to aspects of the redox status of the cell. The combination of a fluorophore in close proximity to the spin of a nitroxide leads to substantial quenching of emission of the fluorophore. We coined the term "pro-fluorescence" [12,13] to describe this effect, by analogy with the "pro-drug" terminology widely used in medicinal chemistry and which reflects how metabolism and chemical conversion reveals the active fluorophore. The probe **2a** contained a widely exploited fluorophore (fluorescein) suitable for the lasers used in confocal microscopy and flow cytometry. It also had a built-in nitroxide that put the spin in close proximity to the fluorophore for maximum quenching [14] and, most importantly, did not allow enzymatic or

spontaneous fluorophore-nitroxide cleavage. However, biological systems, even those compromised by disease, still maintain some degree of redox homeostasis and thus should still able to rapidly reduce the nitroxide moiety present in **2a** and switch on fluorescence. To achieve significant differentiation between normal and stressed cells, it was necessary to interfere with redox homeostasis by adding 2-deoxyglucose to block glycolysis and thus shift the cells to more oxidising conditions. We then added rotenone to block mitochondrial complex I and generate reactive oxygen species (ROS). The subsequent changes in cellular redox balance could be followed by flow cytometry using our pro-fluorescent nitroxide (PFN) probe and allowed us to demonstrate changes in probes status reflecting redox couple changes within the cell.

Recently we [15] and others [16] have introduced further structural changes to antioxidant nitroxides that have been used to intervene in enzyme and neutrophil dysfunction. These changes decrease the rate of reduction and prolong nitroxide lifetime. Specifically, replacement of the four methyl groups that cradle the nitroxide spin with larger, more electron-rich ethyl groups, extends the nitroxide lifetime both *in vitro* [15] and *in vivo* [16]. Building on these ideas, we subsequently developed tetraethylisoindoline nitroxides substituted with carboxy groups [17] and used these to make a fluorescein-based PFN (**2b**, $R_2 = -CH_2CH_3$). While the four ethyl groups in the PFN **2b** convey some advantages over first generation PFN probes, fluoresceins have poor emissivity at low pH and are susceptible to photobleaching. Consequently, an extension to this approach generated a rhodamine analogue (**5**), which could be synthesised from **2b**. Rhodamines are less pH sensitive and less prone to photobleaching. Most importantly, the positive charge on rhodamines leads to their accumulation in mitochondria and this characteristic was further enhanced through the esterification of **5** to give **8**.

The mitochondrion is an important organelle, with a critical influence over the redox status of the cell. Mitochondria are a major focus for drug development, reflecting their key role in a range of pathologies [18-22], as well as being a major site of cellular radical production. A number of nitroxides [23-26] have been described that are targeted to mitochondria. These have mostly involved triphenylphosphonium ions following the early work by Murphy and co-workers [27] suggesting the use of charged lipophilic catiion side-chains to induce enhanced delivery of antioxidants into mitochondria. A notable alternative to this approach has been the elegant methodology of Kagan and Wipf et al. [28, 29], who used peptides based on the

natural product hemigramicidin to induce mitochondrial uptake. To our knowledge, all of the mitochondria-targetted compounds described involve rapidly reduced tetramethyl nitroxides and/or cleavable linkers between the nitroxide and the side-chain.

Accumulation in response to the mitochondrial and plasma membrane potential can lead to the many hundred-fold enhanced concentrations of nitroxides in the mitochondrial matrix [30]. However it is important to note that, no matter the equilibrium position, these probes rapidly shuttle in and out of the mitochondria, with these organelles representing only a proportion of a cell's total volume. Consequently, even mitochondrially-targeted nitroxides are also present in the rest of the cell, where they are subject to differing biochemical processes. One of the challenges for all mitochondrial probes therefore, is managing the response arising from non-mitochondrially localized probes exposed to significantly different chemical environments from those of the mitochondria. To address this, an ideal mitochondria-targeted PFN probe should be less responsive in the cytosol and extra-cellular environment, predominantly switching on inside the mitochondria. The slower reduction of the tetra-ethyl, rhodamine-based nitroxide **5** represents one means to achieve this goal.

Herein we extend our earlier work and report the synthesis and properties of carboxyisoindoline nitroxides and their conversion into redox-responsive fluorescein and rhodamine pro-fluorescent probes that respond in real-time and reversibly to changes in the redox status of certain redox couples in living systems. The presence of bulky ethyl groups limits fluorescence switch-on to highly reducing environments and, in combination with the positively charged rhodamine structure, effectively confines the fluorescence response to within mitochondria. This makes the probes suitable for imaging redox changes within cells for extended periods of time and has implications for developing our understanding of mitochondrial metabolism and pathology.

Materials and Methods

General methods

Reagents and probes

MitoTracker Green, LysoTracker Blue, MitoSox and Hoechst 33258 were supplied by Molecular Probes. All solvents used were Analytical Reagent (AR) grade and all

other chemical reagents were of Laboratory Reagent (LR) quality or better and were used as supplied by the manufacturer.

Preparation of compounds

Analytical thin-layer chromatography (TLC) was performed using Merck Silica Gel 60 F_{254} TLC plates. Preparative column chromatography was performed using Merck Silica Gel 60 (mesh 230-400). Mass spectra were recorded using a Bruker Apex 3 Fourier transform ion cyclotron resonance mass spectrometer with a 4.7 T magnet. Analytical HPLC was performed on a Hewlett Packard 1100 series HPLC, using an Agilent prep-C18 scalar column (10 μ m, 4.6 × 150 mm) at a flow rate of 1 mL/min. Fluorescence spectra were obtained using either a Varian Cary Eclipse fluorescence spectrophotometer (Agilent Technologies, USA) equipped with a standard multi-cell Peltier thermostatted sample holder, or a Shimadzu RF-5301PC fluorescence spectrophotometer (Shimadzu Scientific Instruments Inc., Japan) equipped with a magnetic stirrer.

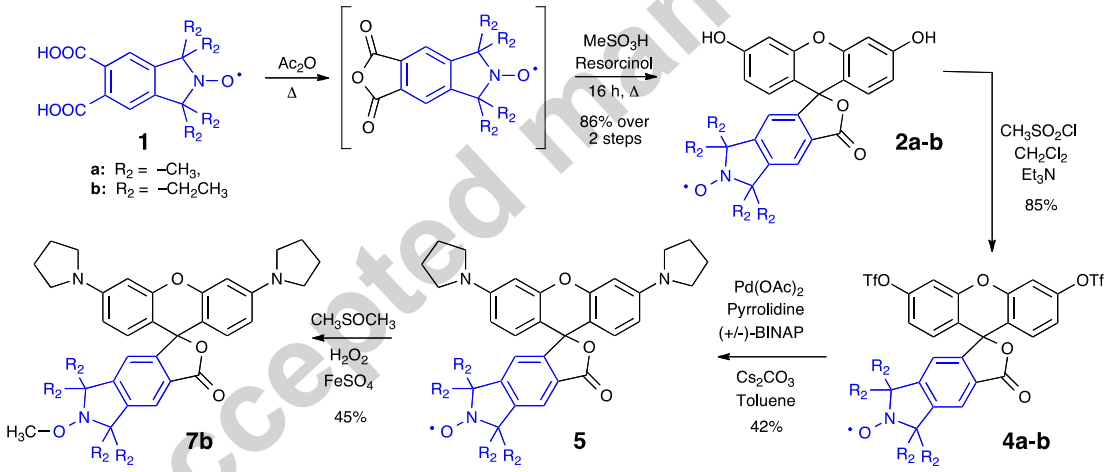

Scheme 1. Carboxyisoindoline nitroxides (**1**) are converted to fluorescein-based pro-fluorescent nitroxides (**2**) and rhodamine-based nitroxides (**5**). Nitroxides such as **2** and **5** may be permanently converted to the close structural, but non-radical, methoxyamine analogues (**7b**) by treatment with iron and hydrogen peroxide in dimethylsulfoxide.

*Synthesis of tetramethyl and tetraethyl nitroxides (***1a-d***)*

These nitroxides were synthesised following procedures described by Fairfull-Smith et al. [17] and references therein.

Synthesis of tetramethylfluorescein nitroxide (**2a**).

This probe was synthesised following the method described by Morrow et al. [11]

Synthesis of tetraethylfluorescein nitroxide (**2b**).

5,6-Dicarboxy-1,1,3,3-tetramethylisoindolin-2-yloxyl (**1b**) (150 mg, 0.45 mmol) was dissolved in acetic anhydride (Ac_2O, 3 mL) and heated for 1 hr at 95°C. The solution was returned to room temperature and the acetic anhydride was removed by distillation under reduced pressure to give an orange solid. This solid was taken up in methane sulfonic acid ($MeSO_3H$, 1.5 mL) and resorcinol (99 mg, 0.90 mmol, 2 equiv) was added. The mixture was heated at 85°C for 16 hr before being poured onto ice. NaOH (5 M) was carefully added to dissolve the precipitate and the solution was stirred for 15 min. The solution was cooled to 0°C and acidified with HCl (conc.). The resultant brown precipitate was filtered and thoroughly washed with cold H_2O and dried under high vacuum. Purification of the crude product by flash column chromatography (5 % MeOH / 95 % $CHCl_3$) gave an orange powder (193 mg, 86 %); +EI MS found 500.2082 (1.8 ppm from calc. mass of $C_{30}H_{30}NO_6^{\bullet}$); *m/z* 500 ($M^+$, 100 %), 472 (35), 446 (15), 427 (25), 411 (32); found: C, 71.82; H, 6.11; N, 2.89. $C_{30}H_{30}NO_6^{\bullet}$ requires C, 71.98; H, 6.04; N, 2.80.

Synthesis of tetramethylfluorescein triflate nitroxide (**4a**).

To a solution of the fluorescein nitroxide (**2a**, 50 mg, 0.112 mmole) in DCM (0.15 mL), triethylamine (Et_3N, 34 μL, 2.44 mmole, 2.2 equiv.) was added and stirred at 0°C for 5 min whereupon trifluoromethanesulfonyl chloride was added (42 mg, 26 μL, 0.772 mmol, 2 equiv.) The mixture was allowed to return to room temperature and stirred over a period of 6 hr. A volume of DCM (~20 mL) was added to the reaction mixture, and the organic phase was washed with 2 M HCl (2 × 40 mL) and brine (20 mL). The DCM extract was dried over Na_2SO_4 and the solvent was evaporated under reduced pressure. The crude material was purified by flash chromatography (SiO_2, 98% DCM/2% acetone) to give the triflate derivative as a white solid (67.4 mg, 85 %). +ESI HRMS found $(M+H)^+$ 709.05055 (0.8 ppm from calc. mass of $C_{28}H_{21}NO_{10}F_6S_2$.

Synthesis of tetraethylfluorescein triflate nitroxide (**4b**).

Trifluoromethanesulfonyl chloride (152 mg, 96 μL, 0.90 mmol, 4 equiv) was added dropwise to a solution of tetraethyl fluorescein nitroxide **2b** (113 mg, 0.23 mmol) and Et_3N (138 μL, 0.99 mmol, 4.4 equiv) in 2 mL of dichloromethane (DCM) at 0°C. The mixture was allowed to return to room temperature over a period of 1 hr. A volume of DCM (~40 mL) was added to the reaction mixture, and the organic phase was washed with 2 M HCl (2 × 40 mL) and brine (40 mL). The DCM extract was dried over Na_2SO_4 and the solvent was evaporated under reduced pressure. The crude material was purified by flash chromatography (SiO_2, DCM) to give the triflate derivative as a pale yellow solid (147 mg, 85 %). Crystals suitable for elemental analysis could be obtained by recrystallisation from hexane (76 mg, 52 % recovery). +ESI HRMS found $(M+H)^+$ 765.1135 (0.3 ppm from calc. mass of $C_{32}H_{29}NO_{10}F_6S_2$) and $(M+Na)^+$ 787.0973 (2.0 ppm from calc. mass of $C_{32}H_{28}NO_{10}F_6S_2Na$); found: C, 50.27; H, 3.76; N, 1.88; S, 8.43. $C_{32}H_{28}NO_{10}F_6S_2^{\bullet}$ requires C, 50.26; H, 3.69; N, 1.83; S, 8.39.

Synthesis of tetraethylrhodamine nitroxide (**5b**).

A Schlenk tube was flame dried under high vacuum and returned to room temperature under a flow of argon. The reaction vessel was charged with $Pd(OAc)_2$ (1.8 mg, 0.008 mmol, 10 mol% Pd), (±)-BINAP (7.3 mg, 0.012 mmol, 15 mol%) and toluene (2 mL). This mixture was stirred for 10 min until a peach-colored suspension had formed. Tetraethylfluorescein triflate nitroxide (**4b**) (60 mg, 0.08 mmol), pyrrolidine (16 μL, 0.18 mmol, 2.4 equiv) and Cs_2CO_3 (72 mg, 0.22 mmol, 2.8 equiv) were then added to the mixture and the vessel was flushed with argon for 10 min. The temperature was raised to 85°C, the vessel was sealed and the reaction mixture was stirred at this temperature for 24 h. A volume of Et_2O (~40 mL) was added to the reaction mixture and the organic phase was washed the HCl (2 M, 3 × 40 mL). The acidic aqueous phase was cooled to 0°C and made basic by the dropwise addition of NaOH (10 M). The product was extracted into Et_2O (3 × 40 mL), the organic phases were combined and subsequently washed with brine and dried over Na_2SO_4. The solvent was removed under reduced pressure and the crude solid was purified by flash column chromatography (solvent gradient from $CHCl_3$ + 0.5 % v/v Et_3N to 90 % $CHCl_3$/10 % MeOH + 0.5 % v/v Et_3N). The purified fraction was isolated as a purple solid (20.1

mg, 42 %). +ESI HRMS found $(M+H)^+$ 607.3413 (0.5 ppm from calc. mass of $C_{38}H_{45}N_3O_4$).

Synthesis of methyl adduct of tetraethylrhodamine nitroxide (**7b**).

Hydrogen peroxide solution (30%, 3.74 uL, 3.30×10^{-5} mol) was added dropwise to a solution of tetraethylrhodamine nitroxide **5b** (10 mg, 1.65×10^{-5} mol) and iron (II) sulphate heptahydrate (9.2 mg, 3.30×10^{-5} mol) in DMSO (1 mL). The resulting solution was stirred at room temperature for 40 min and then diluted with aqueous sodium hydroxide (2.5 M, 10 mL). The mixture was extracted with diethyl ether (3 × 30 mL) and the combined organic layers dried (anhydrous Na_2SO_4) and concentrated *in vacuo*. Purification by silica column chromatography (eluent 0.5% $Et_3N/CHCl_3$ → 0.5% Et_3N/5% MeOH/$CHCl_3$) gave **7b** as a pale pink oil (5 mg, 49%).

Synthesis of tetraethylrhodamine nitroxide methyl ester (**8b**).

Acetyl chloride (200 µL, 2.8 mmol) was added dropwise to a suspension of tetraethylrhodamine nitroxide **5b** (11.2 mg, 1.85 mmol) in anhydrous methanol (1.5 mL). The resulting solution was heated at 50°C for 2 days. The reaction mixture was diluted with water and extracted with EtOAc and $CHCl_3$. The combined organic layers were dried (anhydrous $MgSO_4$) and concentrated *in vacuo* to give **8b** as a sticky pink solid (0.063 g, 55%).

Synthesis of methyl adduct of tetraethylrhodamine nitroxide (**10b**).

Hydrogen peroxide solution (30%, 3.74 uL, 3.30×10^{-5} mol) was added dropwise to a solution of tetraethylrhodamine nitroxide methyl ester **8b** (10 mg, 1.65×10^{-5} mol) and iron (II) sulphate heptahydrate (10 mg, 3.2×10^{-5} mol) in DMSO (1.5 mL). The resulting solution was stirred at room temperature for 40 min and then diluted with brine. The mixture was extracted with $CHCl_3$ (3 × 30 mL) and the combined organic layers dried (anhydrous Na_2SO_4), concentrated *in vacuo* and dried under high vacuum at 35°C to remove all traces of DMSO. The resulting solid was dissolved in water and extracted into DCM. The combined DCM layers were dried (anhydrous Na_2SO_4) and concentrated *in vacuo* to give **10b** as a purple solid (10 mg, 50%).

Attempted synthesis of tetramethylrhodamine nitroxide (**5a**).

Tetramethylfluorescein triflate nitroxide (**4a**) (35 mg, 0.049 mmol), $Pd(OAc)_2$ (1.2 mg, 0.005 mmol, 10 mol% Pd), (±)-BINAP (4.8 mg, 0.008 mmol, 15 mol%), Cs_2CO_3 (45 mg, 0.138 mmol, 2.8 equiv and pyrrolidine (12.5 μL, 0.15 mmol, 3 equiv) were dissolved in anhydrous dioxane (0.1 mL) and heated under argon at 100 °C for 16 h. The reaction was cooled HCl (2 M, 15 mL) was added and the acidic phase was washed with Et_2O (2 x 20 mL). The aqueous phase was removed under reduced pressure and the residue taken up in EtOH (~10 mL). Et_2O was added to help precipitate inorganic salts and the solution filtered and then evaporated to dryness under vacuum. The crude product was partially purified by flash column chromatography (80% EtOAc / 20% EtOH with ~1% Et_3N added to limit streaking) to give purple solid (7 mg, < 25%) which melted with decompositon >300 °C. +ESI HRMS gave a peak $(M)^+$ 551.27916 (1.4 ppm from calc. mass of $C_{34}H_{37}N_3O_4$). However there were other peaks present and HPLC gave a broadened peak reflecting limited purity.

Cell culture methods

Cell lines were maintained in exponential growth as monolayers in Dulbecco's modified Eagle's medium (DMEM) or Advanced DMEM. For neonatal foreskin fibroblasts immortalised with human telomerase reverse transcriptase (NFF hTERT), DMEM was supplemented with 12% foetal calf serum (FCS), and 1% penicillin-streptomycin antibiotics; for DLD-1 colorectal adenocarcinoma cells, 4% FCS, 1% glutamine and 1% antibiotic-antimycotic were used. The cells were incubated under standard culturing conditions at 37°C, with 5% (v/v) CO_2 under humidified conditions. For imaging experiments, phenol red containing DMEM was exchanged for phenol-red free DMEM. NFF hTERT were also regularly tested for mycoplasma contamination using MycoAlert (Lonza) and Hoechst 33258 staining.

Flow cytometry

NFF hTERT were cultured as detailed above to sub-confluent (approximately 2×10^5 cells per mL) and confluent (approximately 6×10^5 cells per mL) levels over a period of 48 h in 6-well plates. Cells were treated with nitroxide probe (**5b**, **6b**: 1 μM. **8b**, **9b**: 5 nM) or MitoSOX^{TM} in complete media at 37°C, 5% CO_2 for 45 min, after which they were washed with PBS and then incubated with various concentrations of rotenone or antimycin for 15 min (F_s). All control wells (F_c) were treated with media

containing vehicle (DMSO). Cells were then detached using trypsin/versene and pelleted via centrifugation at 1200 rpm for 4 min. The supernatant was removed and the cells were resuspended in 1 mL PBS in preparation for flow cytometry using a Becton–Dickinson LSRFortessa Flow Cytometer. All samples were kept in the dark to avoid photobleaching prior to measurement. Between each run, the system was rinsed and cleaned with bleach (70% v/v) to avoid cross-contamination. Probes **5b**, **6b**, **8b** and **9b** were excited with a 561 nm laser and emission was detected using a 582/15 nm filter set. MitoSox™ was excited with a 488 nm laser and emission was detected using a 582/15 nm filter set. Data were collected from a total of 10000 cells per sample. Sample data were gated on acquisition to exclude oversized/doublets and necrotic material. Mean fluorescence intensity values from control (F_c) and treated (F_s) samples were used to calculate the percentage change in fluorescence intensity (% Δ F) after treatment using the following equation:

$$\% \Delta F = \frac{(Fs - Fc)}{100} \times 100$$

Fluorescence microscopy

Fluorescence imaging studies to determine subcellular localisation of nitroxide probes were performed using a Deltavision wide-field microscope (Applied Precision) with an enclosed environmental chamber (37°C, 5% CO_2). Cells were plated into 8-well chamber slides (Ibidi) at a density of 1.5 ×10^4 cells per well (200 μL). The following day, cells were incubated with combinations of nitroxide (**5b**, **6b**: 1 μM or 5 nM. **8b**, **9b**: 5 nM) and various fluorescent probes which target subcellular organelles (1.6 μM Hoechst 33258 (nucleus), 100 nM MitoTracker™ Green (mitochondria) or 50 nM LysoTracker® Blue (lysosomes)). Briefly, incubating medium was replaced with 200 μL of phenol red free complete media containing the dye combinations. Typically, cells were incubated for 45 min at 37°C, 5% CO_2, whereupon they were washed (1×) with 200 μL of phenol red free complete media. Phenol red free complete media was replaced and cells imaged. Hoechst 33258 and LysoTracker® Blue were imaged using a DAPI filter set (Ex: 390/18 nm, Em: 435/48 nm), whilst nitroxides and MitoTracker™ were visualised with Cy3 (Ex: 541/27 nm, Em: 593/45 nm) and FITC filter sets (Ex: 475/28 nm, Em: 523/36 nm), respectively.

Fluorescence spectroscopy

Fluorescence measurements were conducted on a Varian Cary Eclipse fluorescence spectrophotometer fitted with a microplate reader accessory or a Shimadzu RF-5301PC spectrofluorophotometer (Shimadzu Scientific Instruments Inc., Japan) equipped with a magnetic stirrer. Fluorescein nitroxide **2** was excited at 490 nm, and the emission was detected at the peak around 525 nm or over the range 495–600 nm. Reduction reactions with ascorbate and hydrazine were conducted in 0.01 M phosphate-buffered saline, pH 7.4 (PBS). Nitroxide probes **2**, **5** or **8b**, or the methoxyamine derivatives, were added to samples at a final concentration of 1 μM, or less, from a 10 mM stock solution prepared in DMSO or EtOH/PBS. Stock solutions of the probes were stored in a −23 °C freezer until use. As ascorbate in solution can be unstable, reduction experiments were performed using a fresh 0.5 M stock solution of ascorbate prepared for each experiment with appropriate dilutions made to achieve a final ascorbate concentration of 100 μM.

Fluorescence lifetime imaging microscopy (FLIM)

Fluorescence lifetime images were collected on a Leica TCS SP5 MP FLIM system containing a tunable Mai Tai Deep See multi-photon laser with a repetition rate of 80 MHz (Spectra-Physics) connected to a Leica DMI6000B-CS inverted microscope. Samples were illuminated with 820 nm laser and emitted light was collected in the de-scanned internal FLIM detectors over the 550 – 650 nm using a HCPLAPO 63X water-immersion (NA = 1.20) objective lens. The data was collected with the aid of the B&H SPCM software and the fluorescence lifetimes were determined using time correlated single photon counting (TCSPC) and analysed with SPC Image software (version 3.1.0.0). The instrument response function was derived from the decay curve of urea. 512 × 512 pixel images were collected and 3X binning applied for analysis to ensure that at least 1×10^4 photons per pixel were analysed. Each sample was scanned for 120 s. Analysis of fluorescence lifetimes in cells required individually fitted mono or bi-exponential curves to obtain average χ^2 values closest to 1.

Mitochondrial preparations and incubations

Bovine heart mitochondrial membranes were prepared as described [31] and stored at -80°C and incubated at 0.2 mg protein/mL in KCl buffer. Mitochondria were prepared from the hearts of female Wistar rats of 10 to 12 weeks of age (Charles River, UK). Animals were killed by stunning followed by cervical dislocation, and the liver and heart were removed to ice-cold buffer. Rat heart mitochondria were isolated by homogenisation and differential centrifugation at 4°C in buffer containing 250 mM sucrose, 5 mM Tris-Cl, and 1 mM EGTA (pH 7.4) supplemented with 0.1% (w/v) fatty acid-free bovine serum albumin. Protein content of the mitochondrial preparations was determined using the biuret assay with bovine serum albumin as a standard. Mitochondrial incubations were performed in KCl buffer [120 mM KCl, 10 mM HEPES, 1 mM EGTA (pH 7.2)], unless stated otherwise. PFN probes **2b** and **8b** were dissolved in EtOH (1 mg/mL) and diluted in PBS to give final concentrations of 0.2-2.0 μM in a total volume of 3 mL of PBS in a 1 × 1 cm^2 quartz fluorimeter cell loosely capped with a Teflon lid and stirred with a Teflon coated micro stirrer bar at 400 rpm to keep the membranes or mitochondria in suspension.

Results

Antioxidant action and bio-availability of tetra-methyl vs tetra-ethyl carboxy isoindoline nitroxides

The original pro-fluorescent fluorescein nitroxide (**2a**) was derived [11] from the dicarboxytetramethylisoindoline nitroxide **1d**. The carboxy nitroxide CTMIO (**1a**) is a tetra-methyl nitroxide and such species, along with related antioxidants, have efficacy in cells and *in vivo* [32-39]. Recent attention has focused on more structurally hindered tetra-ethyl analogues [16], with the hope of enhancing activity by limiting bio-reduction [8]. However, the replacement of the methyl groups in CTMIO (**1a**) with ethyl groups (to give **1c**), gives a compound that is insoluble in water. Introduction of an extra carboxyl group [40] gave the more soluble tetra-ethyl dicarboxy analogue DCTEIO (**1b**) that was a more effective antioxidant than the CTMIO parent [41].

Hence here we focused on converting dicarboxy tetraethyl isoindoline nitroxides to fluorophore-containing nitroxides to generate probes that are responsive to specific cellular compartments and conditions. The ethyl groups in **5b** and **8b** should substantially decrease cellular reduction. Notably, the negative reduction

potential of redox couples present within the mitochondria serve to rapidly generate the non-radical fluorescent hydroxylamines (**6b** and **9b**). Consequently the probe is predominantly "switched off" and therefore has low fluorescence emissivity, except in mitochondria. ROS and oxidising species should be able to re-form the nitroxide and therefore the levels of fluorescence from within the mitochondria are expected be responsive to the redox potential of redox couples within this organelle.

Synthesis of tetraethyl nitroxide fluorescein and rhodamine analogues

The synthesis of the tetraethyl nitroxide fluorescein analogue (**2b**) was achieved via the condensation of two equivalents of resorcinol with the anhydride generated from a dicarboxyisoindoline nitroxide, in a manner analogous to our previous synthesis [11] of the tetramethyl analogue **2a** (Scheme 1). The nitroxide anhydride is readily obtained by cyclisation of the dicarboxy nitroxide (**1b** or **1d**) in acetic anhydride, and reaction of this with resorcinol gives a sulfonate ester intermediate (not isolated) that can be reacted with NaOH to produce the fluorescein in the dianion form [11].

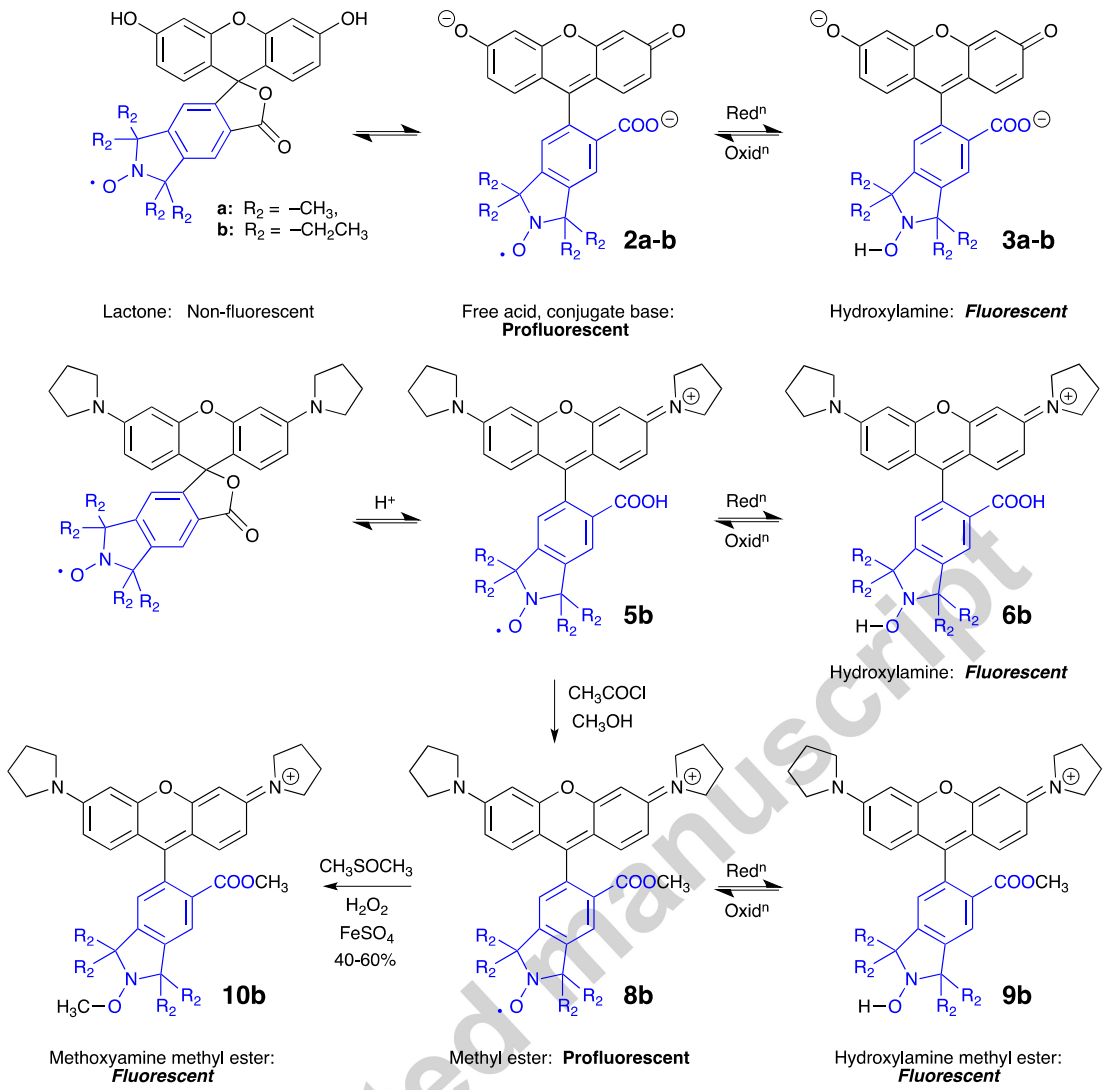

Scheme 2. Synthesis and inter-conversion of fluorescein-based (**2**) and rhodamine-based (**5**, **8**) pro-fluorescent nitroxides and their fluorescent hydroxylamine (**3** and **9**) and methoxamine (**7**, **10**) analogues. (**a** Series $R_2 = CH_3$, **b** Series $R_2 = CH_2CH_3$)

The *ortho* dicarboxy substitution in the ring of the starting materials (such as **1b**), allows access to fluoresceins in good yield in a simple one pot procedure. Fluoresceins may also be converted to rhodamine derivatives via palladium-catalysed Buchwald-Hartwig amination to exchange the phenolic hydroxyl groups with secondary amines. This was achieved by first converting the –OH groups to triflates (in this case **4a** and **4b**) followed by Pd-catalysed amination with pyrrolidine to give the pyrrolidinorhodamine nitroxides as the chloride salt.

As the fluorescence response of fluorescein is pH dependent and can be bleached by the light sources used in microscopy, we focused on the rhodamine

analogues. Product **5b** was of most interest because the tetraethyl analogues possess enhanced stability towards bio-reduction. Furthermore, rhodamines are known to accumulate in mitochondria, driven by the membrane potential. The nitroxide **5b** can be further derivatised to give the methoxyamine **7b** as a positive control for fluorescence experiments with **5**, as they should display similar localisation and transport as the pro-fluorescent nitroxide probes, but they are permanently fluorescent and unaffected by the redox environment.

Comparison of reduction rates of tetra-methyl vs tetra-ethyl probes by ascorbate

To assess the comparative rates of reduction for the fluorescein and rhodamine probes (**2a**, **2b** or **5b**) their reaction with ascorbate was monitored over time (Figure **2**). The reaction of ascorbate with the tetra-ethyl analogues is significantly slower (~10-fold), as indicated for fluoresceins **2a** and **2b**, in Figure **2** and reflecting the slower ascorbate reduction of the parent tetraethylisoindoline nitroxides (0.081 $M^{-1}{\cdot}s^{-1}$) versus the tetramethyl system (0.74 $M^{-1}{\cdot}s^{-1}$) [42]. The tetra-ethyl rhodamine **5b** displayed no apparent reduction over this time period (data not shown). Thus, the reduction of tetraethylnitroxides by ascorbate is slow compared to the methyl analogues (**2a** vs **2b**) and not detectable for the tetraethylnitroxide/rhodamine analogue **5b**.

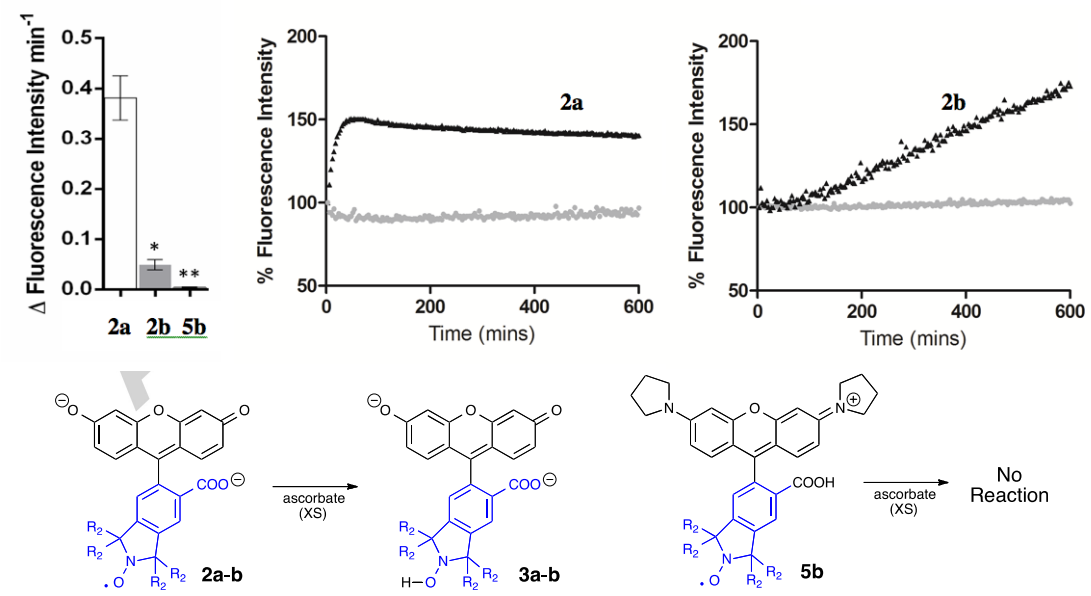

Figure 2. Comparative reduction rates by excess ascorbate of the fluorescein (tetra-methyl) nitroxide probe **2a** compared to the tetra-ethyl analogue **2b**. Blanks with no ascorbate addition are also displayed (lower light grey data points), showing no increase in fluorescence over this time, with the tetra-ethyl analogue **5b** results being indistinguishable from the blank. A 0.5 µM concentration of fluorescein or

rhodamine probes (**2a**, **2b** or **5b**) was prepared in 4 mL PBS and argon was bubbled through the solution to lower oxygen levels. Reduction was initiated by the addition of 375 µM ascorbate (> 750 molar excess). Fluorescence intensity was monitored over time (600 min) and the relative reduction rates were determined based on the slope of the graph of percentage fluorescence intensity changes against time.

*Reduction of fluorescein and rhodamine probes **2b** and **8b** by mitochondrial membranes*

To determine whether biological systems could be more potent at reducing these nitroxides than ascorbate, we incubated them with isolated mitochondrial membranes (Figure **3**). When the membranes were supplied with the respiratory substrate succinate, the conversion of the nitroxides **2b** and **8b** to the more fluorescent hydroxylamines could be observed (Figure **3A** and **B**). Under these conditions, succinate will be oxidised by succinate dehydrogenase and thereby pass electrons on to the coenzyme Q pool and to all respiratory chain carriers between CoQ and oxygen, hence nearly all possible sites of reduction of nitroxides within the mitochondrial respiratory chain will be supplied with electrons and could in principle act as the site of reduction.

A

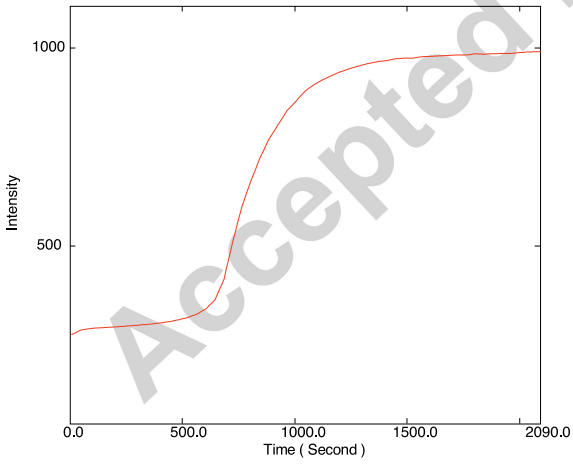

B

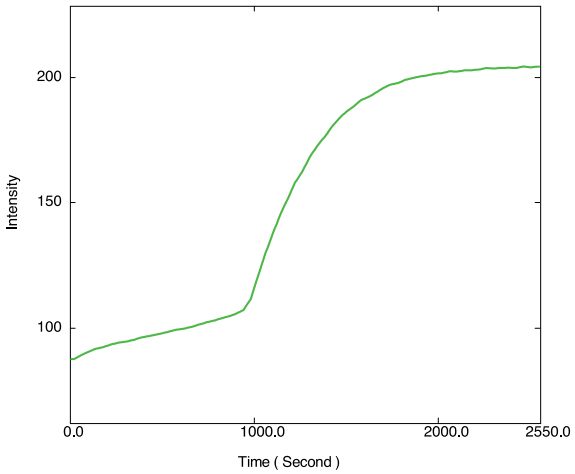

C

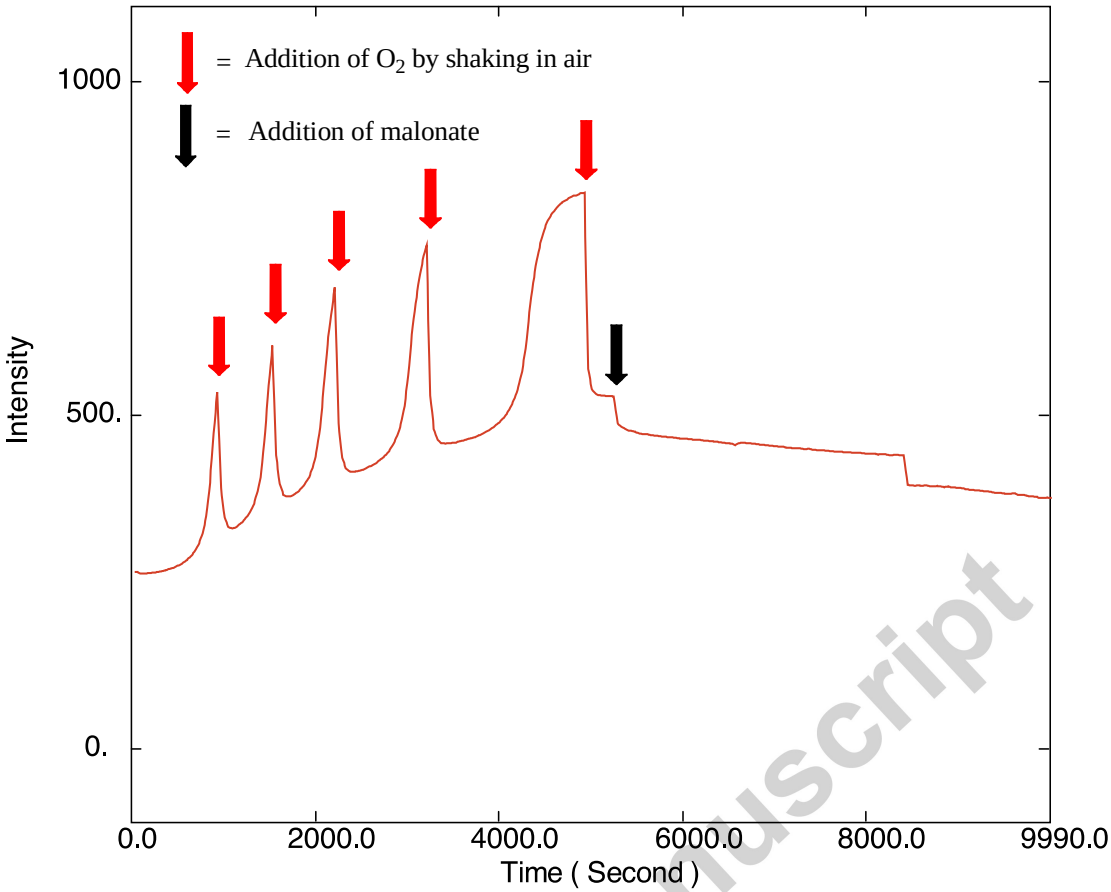

Figure 3. A, B Fluorescence increase over time from fluorescein probe **2b** (Panel **A**. 2.0 μM, 490nm ex. / 520nm em.) and rhodamine probe **8b** (Panel **B**. 0.2 μM, 550nm ex. / 575nm em.) stirred with mitochondrial membranes (0.02 mg) and succinate (6.7 mM) in buffer (3.0 mL). Panel **C** shows the fluorescence increase over time from fluorescein probe **2b** (2.0 μM, 490nm ex. / 520nm em.) stirred with mitochondrial membranes and succinate in buffer in a capped fluorimeter cell. Red arrows indicate when the cap was removed and the mixture aerated by shaking for 10 s.

A lag period before the fluorescence increase occurred was evident and its duration was proportional to the amount of dissolved oxygen present in the closed cell, as the lag period could be shortened by bubbling with argon. Together, these data suggest that the rapid respiration of the mitochondrial membranes depleted the oxygen and enabled reduction of the nitroxide. This was supported by the fact that the lag period lengthened when the cell was stirred rapidly when open to the air to enhance diffusion of oxygen into the suspension. The role of dissolved oxygen in converting the fluorescent hydroxylamine **3b** to the less fluorescent nitroxide **2b**, was further confirmed by an experiment where respiration by the membranes was allowed to deplete the dissolved oxygen and then the fluorimeter cell was re-aerated by shaking with air for 10s. Figure **3** shows the reversible fluorescence response

generated in this experiment. To confirm that the reduction process required electrons supplied by succinate, we added malonate, a competitive inhibitor of succinate dehydrogenase, which prevented the reduction of the nitroxide.

When whole mitochondria were used instead of mitochondrial membranes, the fluorescence switch-on was much greater for the rhodamine based probe, which correlates to the greater uptake expected for a positively charged rhodamine **8b** over the neutral/negatively charged fluorescein **2b** (Figure **4**).

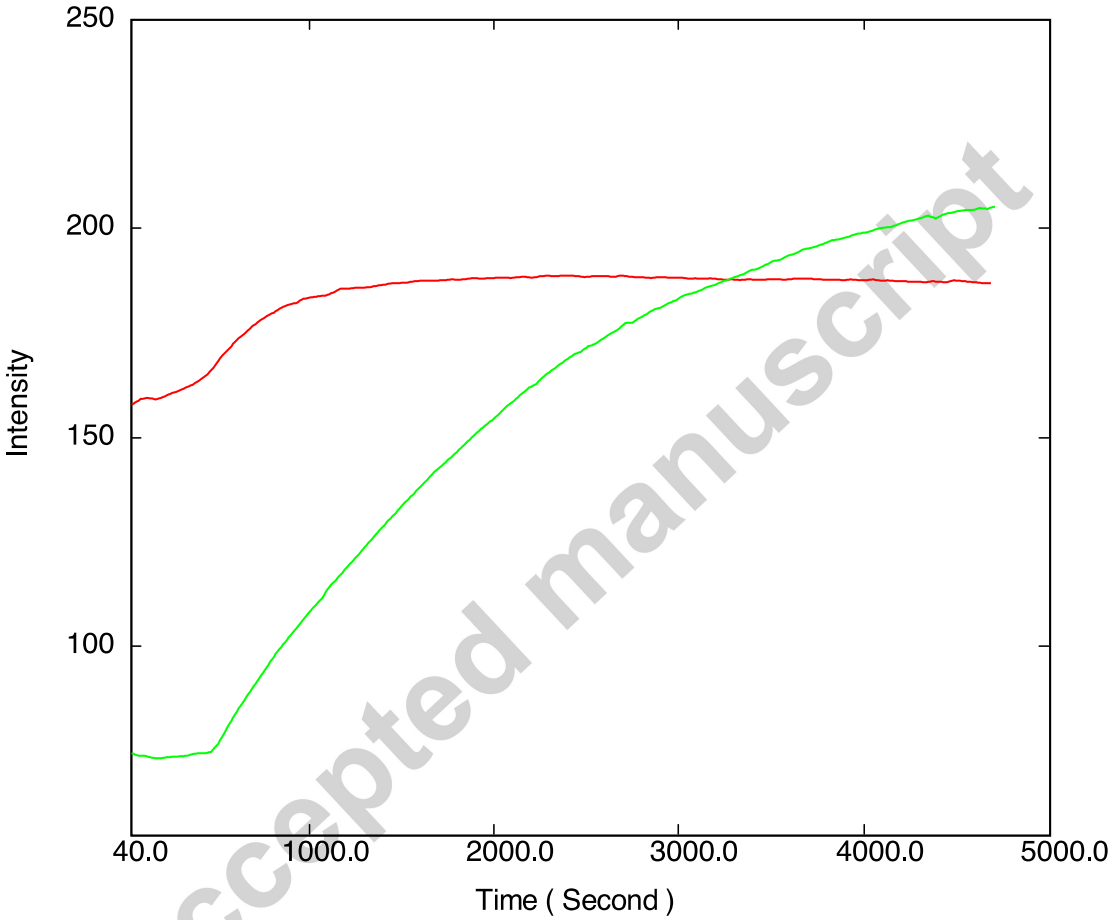

Figure 4. Fluorescence increase over time (75 min.) from fluorescein probe **2b** (Red line, 0.12 μM, 490nm ex. / 520nm em.) and rhodamine probe **8b** (green line, 0.2 μM, 550nm ex. / 575nm em.) exposed to whole mitochondria in the presence of succinate (6.7 mM) in buffer (3.0 mL), open to the air, with RT stirring in a quartz fluorimeter cell.

The same reversible cycling behaviour could be demonstrated for the tetraethyl rhodamine nitroxides (see SI Figure **SI3**), although more demanding redox conditions are required as expected from the limited degree of reduction arising from treatment with excess ascorbate.

These data are consistent with nitroxide reduction by mitochondrial reductive processes that are supplied with electrons by succinate and that the lipophilic cation

character of the rhodamine-based probes enhances the uptake of this molecule into mitochondria.

*Visualising the localisation of the rhodamine nitroxide **5b** in mitochondria within cells*

Simple co-localisation experiments demonstrate that the tetrethylrhodamine nitroxide **5b** predominantly localises within the mitochondria. An overlaid image for cells treated with **5b** and MitoTracker Green (Figure **5C**) supports such mitochondrial localisation. There is evidence for a slightly broader distribution for **5b** than for MitoTracker Green, as images also show some rhodamine fluorescence from within globular structures that were not evident with MitoTracker Green treatment. SoftWorx image analysis was used to determine a coefficient of correlation co-localisation plot (Figure **5D**) which shows how the two emissions (from **5b** and MitoTracker Green) correlate on a pixel-by-pixel basis (where each spot represents a pixel). Based on these images, a co-localisation value of 0.7269 was obtained indicating that most of the **5b** follows the same distribution as MitoTracker Green.

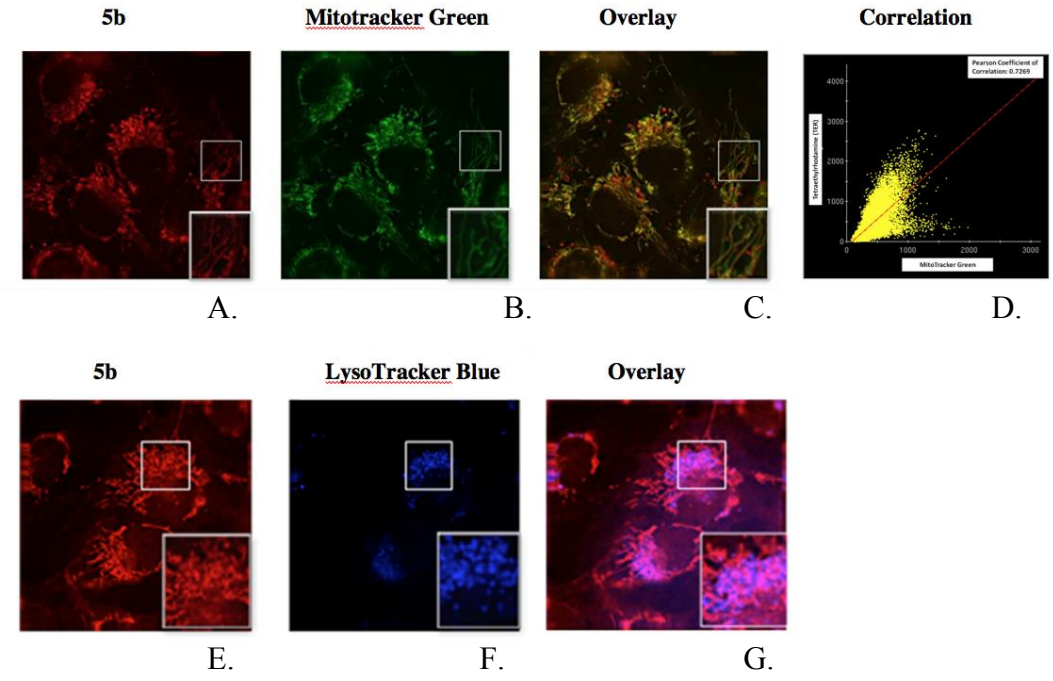

Figure 5. Co-localisation experiments with MitroTracker Green and LysoTracker Blue with the rhodoamine nitroxide probe (**5b**) in hTERT immortalised human fibroblast cells. Panel A: Probe **5b** (1 μM) with insert highlighting typical filamentary mitochondrial structures. Panel B: MitoTracker Green (100 nM). Panel C: Overlay **5b** and MitoTracker Green. Panel D: Correlation plot for overlaid image. Panel E: Probe **5b** (1 μM) with insert highlighting globular bodies possibly reflecting excretion into lysomes / endosomes. Panel F: LysoTracker Blue (50 nM). Panel C: Overlay **5b** and LysoTracker Blue.

An overlaid image from cells treated with **5b** compared to LysoTracker Blue treated cells (Figure **5G**) indicates some localisation of the rhodamine probe to lysosomes with the other globular structures, possibly endosomes. Notably, there is limited fluorescence arising from the cytoplasm. This fluorescence behaviour correlates with **5b** only reaching detectable fluorescence levels on uptake into the mitochondria, where it is reduced to the more fluorescent hydroxylamine (**6b**). Some subsequent excretion of **6b** would account for fluorescence arising from endosomes and lysosomes.

Cells treated with the rhodamine probe **5b** were subsequently treated with either rotenone or antimycin, thereby interrupting the mitochondrial electron transport chain, blocking the supply of electrons to potential reducing sites and also giving rise to higher levels of oxidants. This would be expected to tilt the redox balance towards a more oxidising environment and thereby decrease the overall fluorescence generated. Decreased fluorescence would arise from diminished mitochondrial reduction of **5b** and because some of the hydroxylamine **6b** would be re-oxidised back to **5b**. Flow cytometry was used to monitor cells treated with **5b**, which confirmed that lower fluorescence arises in a dose responsive manner to mitochondrial inhibition (Figure **6B**). The redox responsive probe MitoSox was used as a positive control (Figure **6C**) and demonstrated a dose dependent response to both rotenone and antimycin, reflecting enhanced oxidising conditions in the mitochondria arising from inhibition. The methoxyamine **7b** was used as a negative control (Figure **6D**) and this non-redox active analogue showed no dose-dependent changes in fluorescence. Taken together, these results support the concept that the hydroxylamine/nitroxide ratio controls the probe brightness. Inhibitors that deliver conditions producing increased levels of ROS and stronger oxidation driven switch-on of MitoSOX, tilt the balance towards the nitroxide and lead to a decrease in the fluorescence response detected from cells treated with the rhodamine PFN probe **5b**.

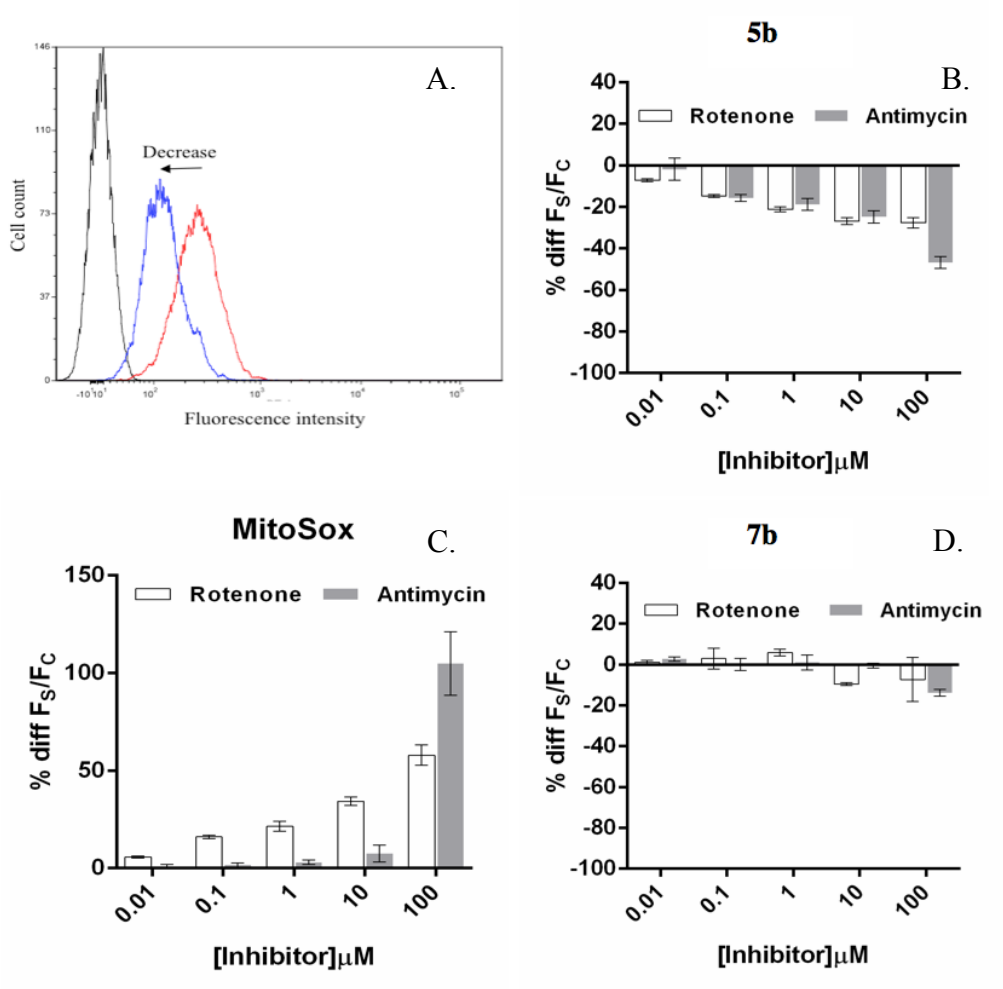

Figure 6. Percentage reduction in fluorescence intensity of treated hTERT immortalised human fibroblast cells, F_s [cells incubated with rhodamine nitroxide **5b** (1 μM) for 45 min, followed by treatment with varying concentrations of rotenone (ROT) or antimycin (AMC)] for 15 min relative to blank, F_c [cells incubated with 1 μM probes for 45 min, followed by treatment with DMSO for 15 min]. **Panel A:** Cells treated with 1 μM **5b** measured by flow cytometry. **Panel B**: Percentage reduction in fluorescence intensity of cell populations incubated with **5b** and treated with 5 doses of 2 inhibitors. **Panel C:** Cells treated with 1 μM MitoSox. **Panel D**: Percentage change in fluorescence intensity for **7b** treated cells with 5 doses of two inhibitors. The results in **A** were analysed using Kruskal Wallis test with *post hoc* testing using the Dunn's multiple comparison test. Data in **B and C** were analysed using One-way ANOVA with *post hoc* testing using the Dunn's multiple comparison test. In all cases **A**, **B and C**, treatments showed significant *P values (< 0.05) compared to the blank. Results for the two inhibitors shown in **B** were only significantly different at the highest dose, but were significantly different in all doses indicated in **C**. Data in **D** were not significantly different P values (> 0.05) compared to blank.

The mitochondrial membrane potential provides a driving force to accumulate positively charged species. The rhodamine nitroxide **5b** will be taken up by the mitochondria as the free acid form (RCOOH) that exists in equilibrium with the conjugate base (Scheme 3). This will lead to greater uptake into the mitochondria due to the combined effect of the uptake of the weak acid driven by the pH gradient and the membrane potential on the fixed positive charge [43]

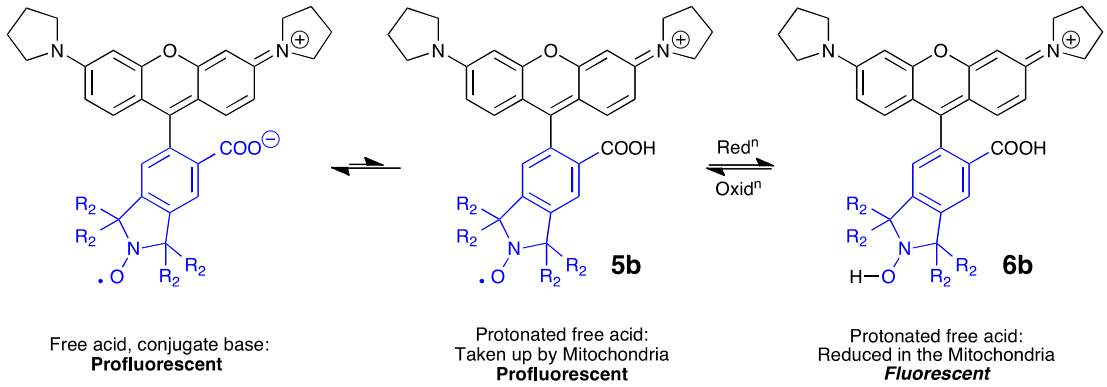

Scheme 3. Small equilibrium concentrations of **5b** present in the RCOOH form (pro-fluorescent, dark), would be driven into the mitochondria by the membrane potential due to the overall positive charge on the molecule. Outside the mitochondria the reduction of the tetraethyl nitroxide probe is slow. Inside the mitochondria the probe would be rapidly reduced and loss of the free radical restores the usual fluorescence emission from the rhodamine fluorophore.

However, the pKa of the carboxylic acid and the consequent significant proportion of the zwitterionic form of either **5b** or **6b** would slow the uptake of the compounds across the plasma membrane. To circumvent this, **5b** was esterified to lock the compound as the permanently positively charged **8b** and also to increase the hydrophobicicty, both of which enhance uptake into the cell and thus provide a stronger fluorescence response driven by mitochondrial action.

There was significantly increased uptake of the rhodamine nitroxide methyl ester **8b** compared to **5b**, enabling us to achieve mitochondrial labelling at much lower incubation concentrations (5 nM of **8b** compared to using 1 μM of **5b**). To further assess the relative uptake, we next studied the redox insensitive non-radical methoxyamine deriviatives (**7b** or **10b**), which have the same fluorescence as the fully reduced probes, and which possess similar physicochemical properties and therefore reflect the fluorescence performance expected when the nitroxide (**5b** or **8b**) is fully reduced to the non-radical hydroxylamine (**6b** or **9b**).

Figure **7** shows that when cells are incubated with the rhodamine probe **5b** using a lower concentration of probe (5 nM), there is negligible detectable fluorescence (Panel A). This was also the case for the methoxamine derivative (**7b**) at this concentration (Panel B). This indicates that, at this concentration, there is insufficient compound taken up into the mitochondria to be detectable under these conditions. However, this was not the case when **8b** was used at the same concentration (5 nM), when there was readily detectable fluorescence within the

mitochondria. Incubation with the fully fluorescent methoxyamine derivative (**10b**) (Panel D) at the same concentration shows the signal that would be expected if all of the nitroxide **8b** was converted to non-radical hydroxylamine **9b**.

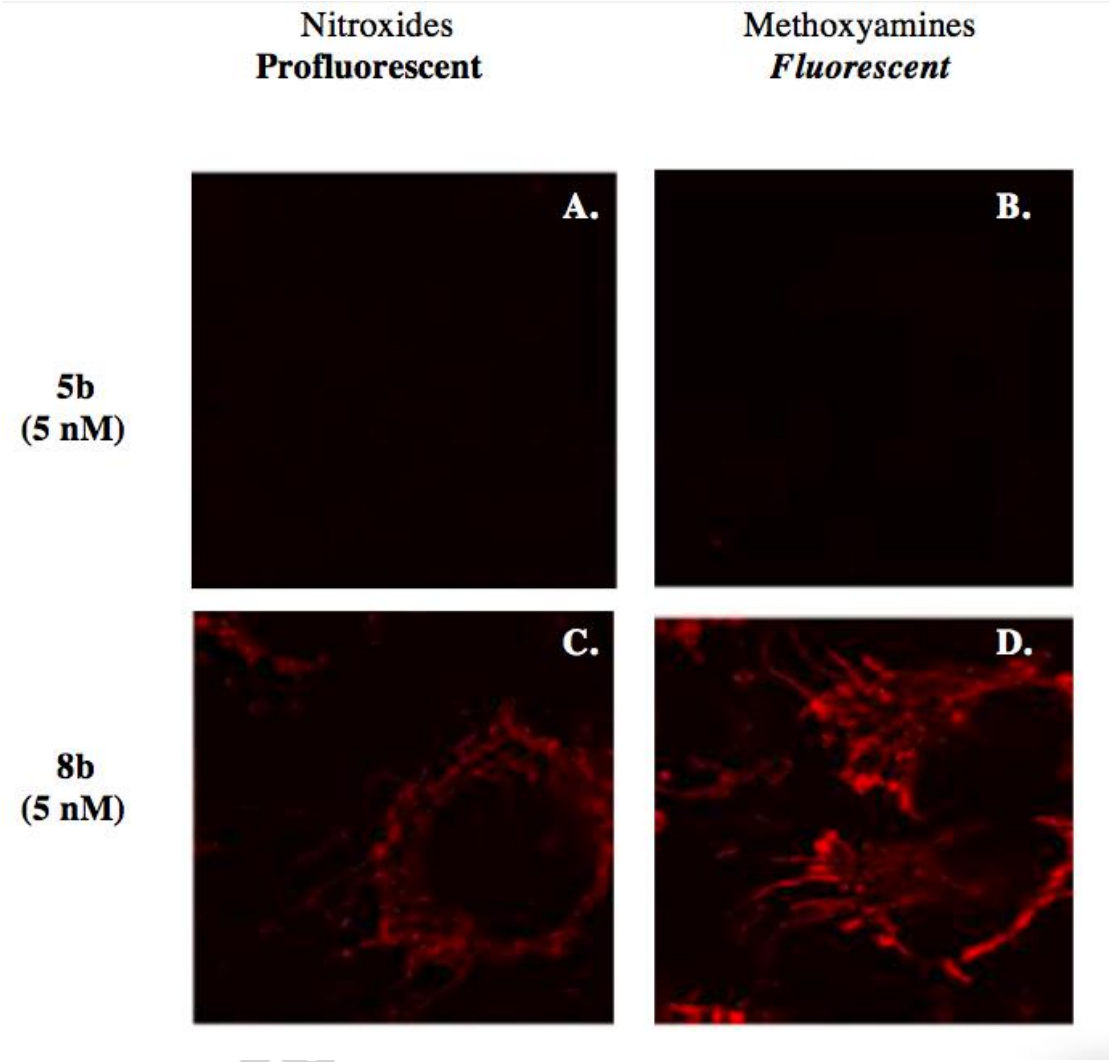

Figure 7. Fluorescence image intensity comparison for very low concentration (5 nM) rhodamine nitroxides and the methyl ester and methoxyamine derivatives in hTERT immortalised human fibroblast cells. Panel A: Rhodamine nitroxide **5b** (5 nM) Panel B: Non-radical methoxyamine (fully fluorescent) analogue (**7b)** (5 nM). Panel C: Rhodamine nitroxide methyl ester (**8b)** (5 nM). Panel D: Non-radical methoxyamine (fully fluorescent) analogue of rhodamine nitroxide methyl ester (**10b)** (5 nM).

A correlation plot for the rhodamine nitroxide methyl ester **8b** and MitoTracker Green (Figure **8**) indicates an increased correlation (0.9217), likely due to the lower concentrations used, which correspond to less induction of excretion pathways.

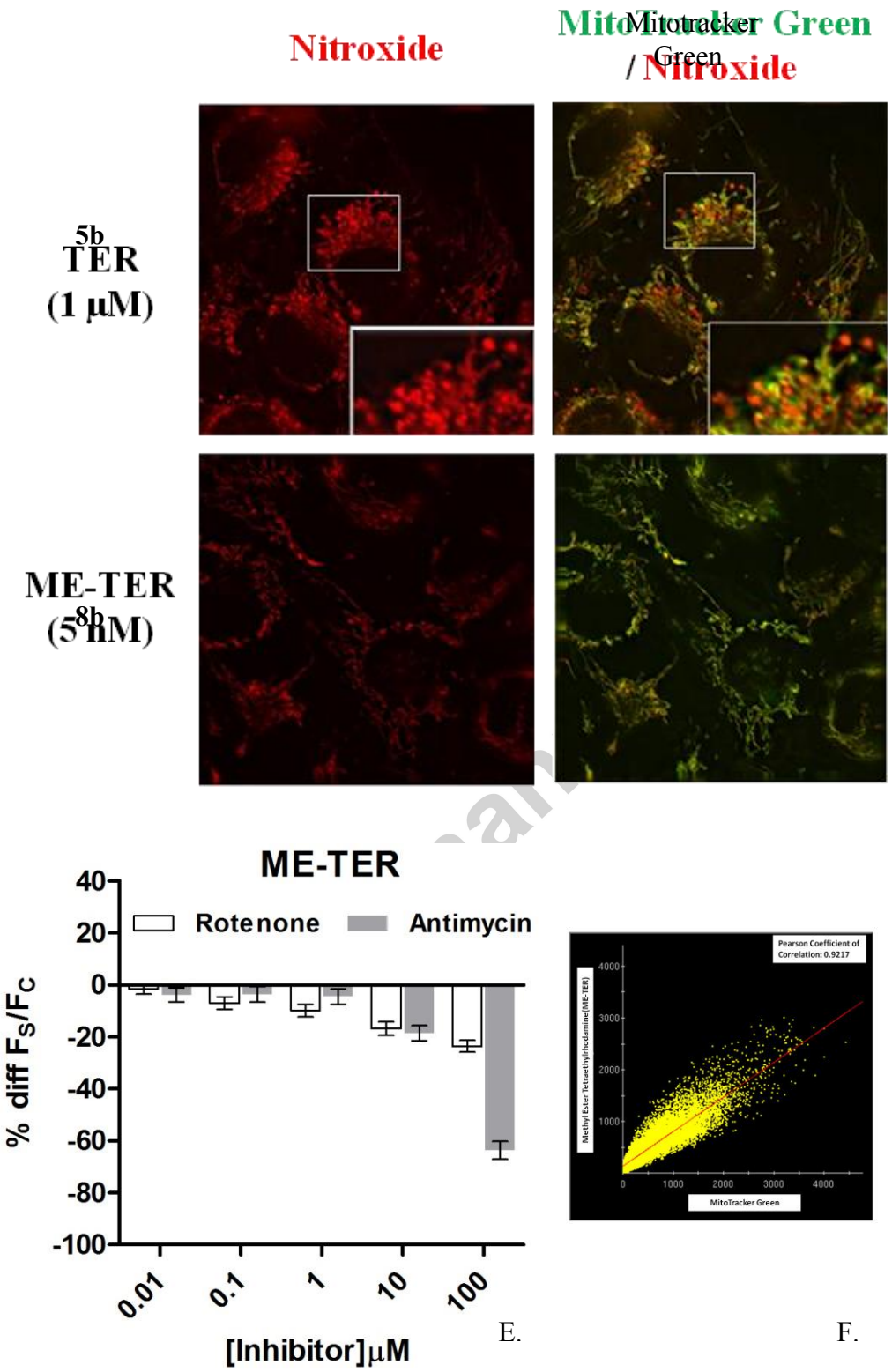

Figure 8. Comparison of the localisation of 1 μM of tetraethylrhodamine nitroxide **5b** (Panel **A**) and 5 nM of methyl ester tetraethylrhodamine nitroxide **8b** (Panel **C**) within hTERT immortalised human fibroblast cells. Co-localisation images of **5b** (1 μM) and **8b** (5 nM), and MitoTracker Green (100 nM) within mitochondria (Panels **B** and **D**). Panel **F** shows the correlation plot and Panel **E** shows the percentage reduction in fluorescence intensity of cell populations incubated with **8b** and treated

with 5 concentrations of the inhibitors rotenone and antimycin. The results shown in **E** were analysed using Kruskal Wallis test with *post hoc* testing using the Dunn's multiple comparison test. Treatments showed significant *P values (< 0.05) compared to the blank.

One of the challenges of applying intensity-based sensors such as pro-fluorescent nitroxides is that emission intensity can be affected by other factors including probe concentration and laser intensity. Ideally the collection of the least ambiguous information requires the use of ratiometric sensing methods, for which spectral changes rather than intensity changes are recorded [44]. Ratiometric sensing is traditionally achieved by using probes that change colour in response to analytes, and to this end Förster resonance energy transfer (FRET)-based ratiometric sensors for cellular redox environment have been developed [45]. However, in theory, any parameter that changes with location can be measured through image mapping methodology that allows the determination of relative ratios. PFNs, with their short fluorescence lifetimes compared to their fluorescent non-radical counterparts, therefore offer an opportunity for lifetime-based ratiometric imaging using fluorescence lifetime imaging microscopy (FLIM). We demonstrate here, for the first time, the power of this technique using **5b**.

DLD-1 colorectal adenocarcinoma cells were treated with **5b** and visualised by confocal microscopy. Cells were then treated with the oxidant hydrogen peroxide or with the inhibitors rotenone and antimycin to disrupt mitochondrial redox balance. By confocal imaging, it was possible to observe a decrease in fluorescence intensity under oxidising conditions, consistent with more probe in the oxidised, pro-fluorescent form (Figure **9A**). Fluorescence lifetime imaging was achieved using two-photon excitation at 820 nm, and all images could be fit to bi-exponential decay with two fluorescence lifetimes, of 1.3 ns and 2.9 ns, corresponding to the pro-fluorescent radical and fluorescent non-radical respectively. Average lifetimes decreased after treatment with oxidants (Figure **9C-F**), consistent with greater proportions of the pro-fluorescent nitroxide radical in these conditions. These average lifetime changes corresponded to changes in the contribution of shorter and longer lifetimes (Figure **9B**): such values are independent of the concentration of the probe, and therefore can be considered to be a ratiometric output.

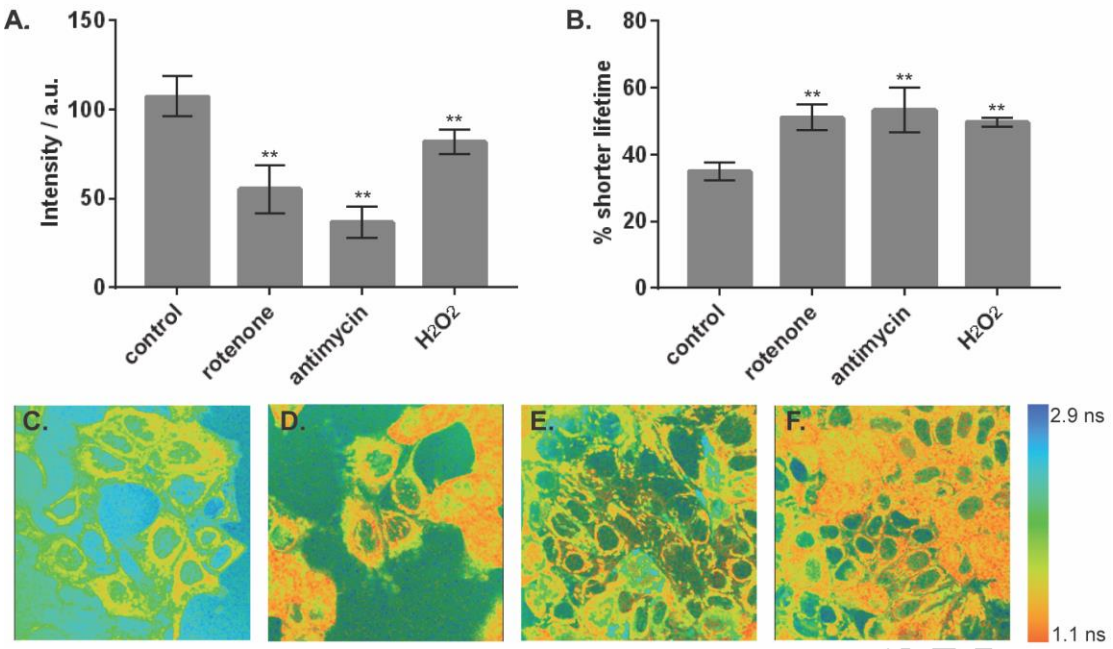

Figure 9: Fluorescence lifetime imaging microscopy enables ratiometric measurement of the proportions of pro-fluorescent radicals and non-radical forms. DLD-1 cells treated with **5b** (100 nM, 15 min) followed by vehicle control, rotenone (10 µM, 15 min), antimycin (10 µM, 15 min) or H_2O_2 (50 µM, 15 min). Panel **A**. Fluorescence intensities from confocal microscope images of cells, 488 nm excitation, 550-650 nm emission. Panel **B**. % shorter (1.3 ns) lifetime from fluorescence lifetime imaging, 820 nm two-photon excitation, 550-650 nm emission. Panels **C**-**F**. Fluorescence lifetime images showing average lifetimes for **C**: control, **D**: rotenone, **E**: antimycin and **F**: H_2O_2. $n = 3$, data reported as mean ± st. dev.

Discussion

Imaging studies for both fluorescein- and rhodamine-based probes over a range of concentrations indicate broad distribution throughout the cell, as well as with higher accumulations in specific cellular compartments. At lower concentration treatments and influenced by exposure times, the fluoresceins are detectable mainly in the membranes and excretory bodies [11]. The fate of the fluorescein probe **2b** taken up by the cell is likely to involve some reduction in the cytosol, but this would be slow compared to the methyl analogue **2a**. It is also likely to involve entry into, and more rapid reduction within, the mitochondria followed by excretion of the resultant hydroxylamine and some amount of re-oxidation by oxygen and other oxidants. The fluorescein **2b** displays highly reversible redox sensitivity in fluorimeter-based studies and flow-cytometry experiments, but is less suitable for confocal microscopy, where photo-bleaching may become an issue.

In contrast, the rhodamines **5b** and **8b** are more robust for confocal imaging and also demonstrate accumulation largely within the mitochondria. There is a greater

degree of "switch-on" of fluorescence within these organelles, as indicated by the fluorescence lifetime experiments (Figure **9**). The esterification of **5b** to give **8b** increases mitochondrial accumulation, such that a detectable fluorescence response can be obtained by cell incubations at concentrations as low as 5 nM, minimising impact on cell and mitochondrial membrane integrity. The reversibility of probe fluorescence is demonstrated by the increase and decrease of fluorescence emission on exposure to mitochondrial membranes and isolated mitochondria followed by exposure to oxygen. In cell imaging studies, the methyl ester probe **8b** shows a significant fluorescence response to antimycin and rotenone treatment, demonstrating that the PFN probes **8b** holds potential as a tool to monitor mitochondrial redox status.

Conclusion

We have shown that dicarboxy nitroxides can be used to generate a new class of redox-responsive probes. These probes provide a real-time and reversible response that enables the monitoring of the mitochondrial redox state within cells and holds promise for the assessment of mitochondrial redox status in cells under a range of conditions.

Acknowledgement

This work was supported by the Australian Research Council Centre of Excellence for Free Radical Chemistry and Biotechnology (CE 0561607) and Queensland University of Technology (KLC, BAC, BJM, KFS, SEB).

References

1. Frémy, E. Nitrosodisulfonate de Potassium. *Ann. Chim. phys*. **15**:408-418; 1845.
2. Piloty, O.; Schwerin, B.G. Ueber die Existenz von Derivaten des Vierwertigen Stickstoffs. *Chem Ber.* **34**:1870-1887; 1901.
3. Lebedev, O. L.; Kazarnovskii, S. N., Intermediate products of oxidation of amines by pertungstate. *Trudy po Khimii i Khimicheskoi Tekhnologii* **2**:649-65; 1959.
4. Hoffmann A.K.; Henderson A.T. A New Stable Free Radical: Di-T-Butyl-Nitroxide. *J. Am. Chem. Soc.* **83**:4671–4672; 1961.
5. Gryn'ova, G.; Ingold, K.U.; Coote, M.L. New Insights into the Mechanism of Amine/Nitroxide Cycling during the Hindered Amine Light Stabilizer Inhibited Oxidative Degradation of Polymers. *J. Am. Chem. Soc* **134**(31):12979-12988; 2012.

6. Samuni, A.; Krishna, C.M.; Riesz, P.; Finkelstein, E.; Russo, A. Nitroxide spin label. A novel metal-free low molecular weight superoxide dismutase mimic. *Journal of Biological Chemistry*. **263**(34):17921-17924; 1988.
7. Mitchell, J.B.; Samuni, A.; Krishna, M.C.; DeGraff, W.G.; Ahn, M.S.; Samuni, U.; Russo, A. Biologically active metal-independent superoxide dismutase mimics. *Biochemistry*. **29**(11):2802-2807; 1990.
8. Keana, J.F.W.; Pou, S.; Rosen, G.M. Nitroxides as potential contrast enhancing agents for MRI application: influence of structure on the rate of reduction by rat hepatocytes, whole lever homogenate, subcellular fractions, and ascorbate *Magn. Res. Med*., **5**: 525-536; 1987.
9. Blinco, J.P.; Hodgson, J.L.; Morrow, B.J.; Walker, J.R.; Will, G.D.; Coote, M.L.; Bottle, S.E. Experimental and Theoretical Studies of the Redox Potentials of Cyclic Nitroxides, *Journal of Organic Chemistry*, **73**(17):6763-6771; 2008.
10. Prescott, C.; Bottle, S.E. Biological Relevance of Free Radicals and Nitroxides, *Cell Biochemistry and Biophysics* **75**(2):227-240; 2017.
11. Morrow, B.J.; Keddie, D.J.; Gueven, N.; Lavin, M.F.; Bottle, S.E. A Novel Profluorescent Nitroxide as a Sensitive Probe for the Cellular Redox Environment. *Free Radic. Biol. Med.* **49**(1):67-76; 2010.
12. Micallef, A.S.; Blinco, J.P.; George, G.A.; Reid, D.A.; Rizzardo, E.; Thang, S.H.; Bottle, S.E. The application of a novel profluorescent nitroxide to monitor thermo-oxidative degradation of polypropylene. *Polym. Degrad. and Stab.* **89**(3):427-435; 2005.
13. Blinco, J.P.; Fairfull-Smith, K.E.; Morrow, B.J.; Bottle, S.E. Profluorescent Nitroxides as Sensitive Probes of Oxidative Change and Free Radical Reactions. *Aust. J. Chem.* **64**(4):373-389; 2011.
14. Lederhose, Paul; Haworth, Naomi L.; Thomas, Komba; Bottle, Steven E.; Coote, Michelle L.; Barner-Kowollik, Christopher; Blinco, James P. Design of Redox/Radical Sensing Molecules via Nitrile Imine-Mediated Tetrazole-ene Cycloaddition (NITEC). *J. Org. Chem.* **80**(16):8009-8017; 2015.
15. Kajer, T.B.; Fairfull-Smith, K.E.; Yamasaki, T.; Yamada, K-I; Fu, S.; Bottle, S.E.; Hawkins, C.L.; Davies, M.J. Inhibition of myeloperoxidase- and neutrophil-mediated oxidant production by tetraethyl and tetramethyl nitroxides. *Free Radic. Biol. Med.* **70**:96-105; 2014.
16. Kinoshita, Y.; Yamada, K.; Yamasaki, T.; Mito, F.; Yamato, M.; Kosem, N.; Deguchi, H.; Shirahama, C.; Ito, Y.; Kitagawa, K.; Okukado, N.; Sakai, K.; Utsumi, H. *In vivo* evaluation of novel nitroxyl radicals with reduction stability. *Free Radic. Biol. Med*. **49:**1703–1709; 2010.
17. Fairfull-Smith, Kathryn E.; Brackmann, Farina; Bottle, Steven E. The Synthesis of Novel Isoindoline Nitroxides Bearing Water-Solubilising Functionality. *Eur. J. Org. Chem.* **12:**1902-1915; 2009.
18. Lewis, W.; Dalakas, M.C. Mitochondrial toxicity of antiviral drugs. *Nature Medicine.* **1**(5):417-22; 1995.
19. Detmer, S.A.; Chan, D.C. Functions and dysfunctions of mitochondrial dynamics. *Nature Reviews Molecular Cell Biology.* **8**(11):870-879; 2007.
20. Fulda, S.; Galluzzi, L.; Kroemer, G. Targeting mitochondria for cancer therapy. *Nature Reviews Drug Discovery*. **9**(6):447-464; 2010.

21. Lyakhovich, A.; Graifer, D. Mitochondria-Mediated Oxidative Stress: Old Target for New Drugs. *Current Medicinal Chemistry* **22**(26):3040-3053; 2015.
22. Garber, K. Targeting mitochondria emerges as therapeutic strategy. *J. Natl. Cancer Inst.* **97:**1800–1801; 2005
23. Trnka, J.; Blaikie, F.H.; Smith, R.A.J.; Murphy, M.P. A mitochondria-targeted nitroxide is reduced to its hydroxylamine by ubiquinol in mitochondria Free Radic. Biol. Med. 44(7):1406-1419; 2008.
24. Desolin, J.; Schuler, M.; Quinart, A.; De Giorgi, F.; Ghosez, L.; Ichas, F. Selective targeting of synthetic antioxidants to mitochondria: towards a mitochondrial medicine for neurodegenerative diseases. Eur. J. Pharmacol. **447:**155-161; 2002.
25. Dhanasekaran, A.; Kotamraju, S.; Karunakaran, C.; Kalivendi, S. V.; Thomas, S.; Joseph, J.; Kalyanaraman, B. Mitochondria superoxide dismutase mimetic inhibits peroxide-induced oxidative damage and apoptosis: role of mitochondrial superoxide. *Free Radic. Biol. Med.* **39:**567–583; 2005.
26. Fink, M.P.; Macias, C.A.; Xiao, J.; Tyurina, Y.Y.; Jiang, J.; Belikova, N.; Delude, R.L.; Greenberger, J.S.; Kagan, V.E.; Wipf, P. Hemigramicidin-TEMPO conjugates: Novel mitochondria-targeted anti-oxidants. Biochemical Pharmacology. **74**(6):801-809; 2007
27. Smith, R. A.; Porteous, C. M.; Coulter, C. V.; Murphy, M. P. Selective targeting of an antioxidant to mitochondria. *Eur. J. Biochem*. **263:**709–716; 1999.
28. Kagan, V.E.; Wipf, P.; Stoyanovsky, D.; Greenberger, J.S.; Borisenko, G.; Belikova, N.A.; Yanamala, N.; Samhan Arias, A.K.; Tungekar, M.A.; Jiang, J.; Tyurina, Y.Y.; Ji, J.; Klein-Seetharaman, J.; Pitt, B.R.; Shvedova, A.A.; Bayir, H. Mitochondrial targeting of electron scavenging antioxidants: Regulation of selective oxidation vs random chain reactions. *Advanced Drug Delivery Reviews* **61**(14):1375-1385; 2009.
29. Wipf, P.; Xiao, J.; Jiang, J.; Belikova, N. A.; Tyurin, V. A.; Fink, M. P.; Kagan, V. E. Mitochondrial targeting of selective electron scavengers: synthesis and biological analysis of hemigramicidin-TEMPO conjugates. *J. Am. Chem. Soc.* **127:**12460–12461; 2005.
30. Kagan, V.E.; Jiang, J.; Bayir, H.; Stoyanovsky, D.A. Targeting nitroxides to mitochondria: location, location, location, and ...concentration. Highlight commentary on "Mitochondria superoxide dismutase mimetic inhibits peroxide-induced oxidative damage and apoptosis: Role of mitochondrial superoxide. *Free Radic. Biol. Med.* **43**(3):348-350; 2007.
31. Dahm, C. C.; Moore, K.; Murphy, M. P. Persistent S-nitrosation of complex I and other mitochondrial membrane proteins by S-nitrosothiols but not nitric oxide or peroxynitrite: Implications for the interaction of nitric oxide with mitochondria. *J. Biol. Chem.* **281**:10056-10065; 2006
32. Reichenbach, J.; Schubert, R.; Schwan, C.; Müller, K.; Böhles, H.; Zielen, S. Anti-oxidative capacity in patients with ataxia telangiectasia. *Clinical and Experimental Immunology,* **117**:535-539: 1999.
33. Gatei, M.; Shkedy, D.; Khanna, K. K.; Uziel, T.; Shiloh, Y.; Pandita, T. K.; Lavin, M. F.; Rotman, G. Ataxia-telangiectasia: chronic activation of damage-responsive functions is reduced by alpha-lipoic acid. *Oncogene,* **20**(3):289-294: 2001.

34. Watters, D.J. Oxidative stress in ataxia telangiectasia. *Redox Reports*, **8**(1): 23-29, 2003.
35. Chen, P.; Peng, C.; Luff, J.; Spring, K.; Watters, D.; Bottle, S.; Furuya, S.; Lavin, M.F. Oxidative stress is responsible for deficient survival and dendritogenesis in purkinje neurons from ataxia-telangiectasia mutated mutant mice. *J Neurosci*, **23**(36):11453-11460; 2003.
36. Gueven, N.; Luff, J.; Peng, C.; Hosokawa, K.; Bottle, S.E.; Lavin, M.F. Dramatic extension of tumor latency and correction of neurobehavioral phenotype in Atm-mutant mice with a nitroxide antioxidant. *Free Radical Biology and Medicine,* **41**(6): 992-1000; 2006.
37. Lam M.A.; Pattison D.I.; Bottle S.E.; Keddie D.J.; Davies M.J. Nitric oxide and nitroxides can act as efficient scavengers of protein-derived free radicals, *Chemical Research in Toxicology*, **21**(11);2111-2119; 2008.
38. Rees, M.D.; Bottle**,** S.E.; Fairfull-Smith, K.E.; Malle, E; Whitelock, J.M.; Davies, M.J. Inhibition of myeloperoxidase-mediated hypochlorous acid production by nitroxides *Biochemical Journal*, **421**:79-86; 2009.
39. Hausler, N.E; Devine, S.M.; McRobb, F.M.; Warfe, L.; Pouton, C.W.; Haynes, J.M.; Bottle**,** S.E.; White, P.J.; Scammells, P.J. *Synthesis and Pharmacological Evaluation of Dual Acting Antioxidant A2A Adenosine Receptor Agonists*, *Journal of Medicinal Chemistry* **55**(7):3521-3534; 2012.
40. Fairfull-Smith K.E.; Brackmann F.; Bottle S.E. The Synthesis of Novel Isoindoline Nitroxides Bearing Water-Solubilising Functionality, *European Journal of Organic Chemistry,* **12**:1902-1915; 2009.
41. Rayner C.L; Bottle S.E.; Gole G.A.; Ward M.S.; Barnett N.L. Real-time quantification of oxidative stress and the protective effect of nitroxide antioxidants, *Neurochemistry International* **92**:1-12; 2016.
42. Jagtap, A.P.; Krstic, I.; Kunjir, N.C.; Hänsel, R.; Prisner, T.F. and Sigurdsson, S. Th. Sterically shielded spin labels for in-cell EPR spectroscopy: Analysis of stability in reducing environment, *Free Radical Research*, **49**(1):78–85; 2015.
43. Finichiu, P.G.; James, A.M.; Larsen, L.; Smith, R.A.J. and Murphy, M.P. Journal of Bioenergetics and Biomembranes **45**:165-173; 2013.
44. Kaur, A.; Haghighatbin, M.A.; Hogan, C.F. and New, E.J. A FRET-based ratiometric redox probe for detecting oxidative stress by confocal microscopy, FLIM and flow cytometry *Chem. Commun.,* **51**:10510-10513; 2015.
45. New, E.J. Harnessing the Potential of Small Molecule Intracellular Fluorescent Sensors *ACS Sens.*, **1**(4):328–333; 2016.

Highlights

- New fluorescent probes give reversible real-time insight into cellular redox status
- Probe structure enhances mitochondrial retention
- Reversible fluorescence switch-on predominantly occurs within mitochondria
- Probe reduction, balanced by re-oxidation, controls fluorophore lifetime and emission

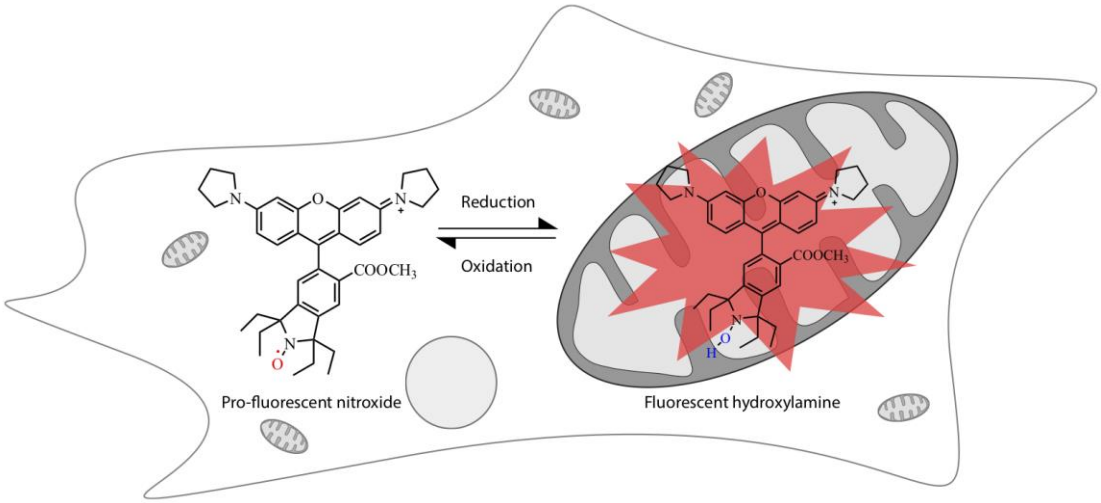

Graphical abstract